JTTEE5 15:413-421
DOI: 10.1361/105996306X124428
1059-9630/$19.00 © ASM International

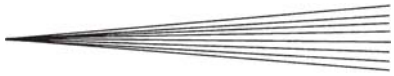

Numerical Modeling of a Low Temperature High Velocity Air Fuel Spraying Process with Injection of Liquid and Metal Particles

X. Yuan, H. Wang, G. Hou, and B. Zha

(Submitted March 29, 2005; in revised form February 27, 2006)

An analysis of a low temperature high velocity air fuel (LTHVAF) thermal spray process is presented using computational fluid dynamics (CFD). The originality of the process lies in the injection of liquid (water) upstream of the powder injection to control the gas temperature and, therefore, the heat transfer to the injected particles. First, computational fluid dynamic techniques are implemented to solve the mass, momentum, and energy conservation equations in the gas phase. A turbulence model based on the renormalized group theory (RNG) is used for the turbulent flow field. The gas dynamic data are, then, used to model the behavior of the liquid droplets and particles in the gas flow field. The calculated results show that the liquid flow rate should range between 20 and 30 kg/h to achieve the optimal gas characteristics for particle treatment. They also show that particle velocity and temperature are strongly affected by particle size. At the gun exit, the particle velocity and temperature range between 700 and 300 m/s and between 900 and 400 K, respectively, for Cu and Ni particles with size distributions of 1 to 50 μm. As expected, the smaller particles have higher velocity and temperature. The metal coatings (Nickel and copper) produced by the LTHVAF spray process are characterized by low oxide content, low residual stresses, high deposition rates, and good bonding to the substrate.

Keywords computational fluid dynamics, copper coatings, high-velocity air fuel (HVAF), nickel coatings, particle behavior

1. Introduction

The high-velocity oxygen-fuel (HVOF) thermal spray process was developed in the 1980s (Ref 1) and expanded rapidly. Later and at the same time, the high-velocity oxygen-air fuel (HVO-AF) and the cold spray processes were developed. The former combines the HVOF and HVAF processes and is characterized by a flame temperature and velocity variable in a rather large range and, thus, makes it possible to increase the variety of the sprayed materials (Ref 2-4). The cold spray technique exhibits a high deposition rate and may also be used to deposit metals, alloys, and composites (Ref 5-7).

In both thermal spray and cold spray processes, the coatings performances depend, to a great extent, on the velocity, temperature, and size of the particles at impact on the substrate. Therefore, the manufacturing of coatings of good quality or any improvement of the spray efficiency require a detailed understanding of the jet flow and its interactions with the sprayed particles.

The particles must exchange momentum and heat with the gas flow to accelerate and heat. As it is well known, the main difference between the thermal spray and cold spray processes lies in the characteristics of the gas that heats and accelerates the particles as the gas temperature in thermal spraying is much higher than in cold spraying. So a question may arise: If the gas temperature in thermal spraying decreases to the same level as in the cold spray process, what will happen? Can oxide-free, dense metal coatings be achieved?

Among the traditional thermal spray processes; the HVAF process can exhibit high velocity with low temperature thanks to an additional device (Ref 8). The technique is based on the HVO-AF spraying system with the injection of a liquid upstream of the powder injection. This innovative process has characteristics close to that of the cold spraying process (Ref 8). A schematic diagram of the low temperature high velocity air fuel (LTHVAF) spraying gun and nozzle is shown in Fig. 1. The spraying conditions are given in Table 1 and the principle of the carrier liquid controller used to produce the liquid jet injected in the gas jet is illustrated in Fig. 2.

Numerical simulations of gas and particle flow through the HVOF spray gun have already been well documented. The more recent papers use three-dimensional CFD-analysis with a coupling between particles and gas flow through the exchange of momentum and energy (Ref 7, 9-12). For instance, the work of K. Sakaki (Ref 7) deals with a model that makes it possible to investigate the effect of the entrance geometry of the gun nozzle for the HVOF spray process. Another work by P.E. Nylén (Ref 12) includes the computational fluid dynamics analysis of gas and particle flow in flame spraying with a detailed description of the physical and chemical processes involved. However, until now, none of the models presented in the literature have dealt with the low temperature velocity air fuel process.

Xiaojing Yuan and **Hangong Wang,** Surface Engineering and Technology, Xi'an Research Institute of Hi-Tech, Xi'an, Shaanxi Province, 710025, China; and **Genliang Hou** and **Bailin Zha,** Surface Engineering and Technology, Xi'an Research Institute of Hi-Tech, Hongqing Town, Xi'an, Shaanxi Province, 710025, China. Contact e-mail: yxj2003@263.net.

Nomenclature

p	pressure
t	time
μ	dynamic viscosity
x	location
S_u,S_E	user-defined source terms
H	total enthalpy
k	kinetic energy per unit mass
Pr	Prandtl number
α	empirically determined constant
A_e	atomizer exit area
C_d	drag coefficient
ρ_g	gas density
T	temperature
m_p	particle mass
c_p	particle heat capacity
A_p	particle surface area
h	convective heat transfer coefficient
ε_p	particle emissivity (dimensionless)
δ	Stefan-Boltzmann constant
θ_R	radiation temperature
d_p	particle diameter
k_∞	thermal conductivity of the continuous phase
Re_d	Reynolds number based on the particle diameter and flow-particle relative velocity
T_p	particle temperature
$c_{p,\infty}$	gas heat capacity
ρ_p	droplet density
k_∞	thermal conductivity of the gas
Nu	Nusselt number

Subscript

p	particle
g	gas

In this paper, a three-dimensional computational analysis of the LTHVAF spraying process with a mixture of kerosene and air, and simultaneous injection of liquid (water), and metal (Ni and Cu) particles is presented and compared with measurements. The objective of the work is to develop a tool to study the effect of gun operating parameters on particle behavior and establish the optimal spraying parameters.

2. Numerical Model

The following modeling strategy is used: (1) the computational fluid dynamic techniques are implemented to solve the mass, momentum, and energy conservation equations in the gas phase; (2) the gas dynamic data are, then, used to model the behavior of the water droplets in the gas fields; (3) the Cu and Ni particles considered as Lagrange entities that exchange momentum and heat with the gas phase, are injected in the gas mixture.

The model developed in this study is based on the following main assumptions:

- The geometry of the spray process is simplified according to the scheme of Fig. 3.

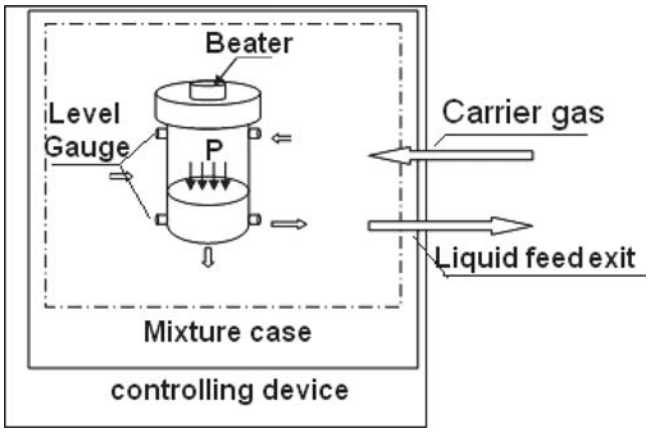

Fig. 2 Schematic of the liquid case. When the water jet enters the gas jet, the latter breaks up the water jet into droplets.

- The combustion gases behave as ideal compressible gases.
- The combustion gas flow in the nozzle is a quasi-one-dimensional isentropic flow of semiperfect gas.
- The profiles of gas velocity, temperature, and pressure are imposed at the entrance of the combustion chamber.
- The heat transfer between the combustion gas and the chamber wall is taken into account.
- The sprayed particles are spherical with negligible internal temperature gradient.
- The particle specific heat is constant.
- The metal particles and water droplets do not exchange mass with the gas phase and do not participate in any chemical reaction.
- The particle temperature is below the material melting point.

2.1 Gas Flow Model

Although the main chemical compounds in the combustion chamber are CO_2, H_2O, O_2, and N_2 (Ref 4), the combustion process is based on the non-premixed probability density function (PDF) distribution model with non-adiabatic previous expansion.

The governing equations of the model are the conservation equations of mass, momentum, and energy for a viscous, compressible, and turbulent flow. The volume fraction of the particulate phase is assumed negligible and a one-way coupling between the gas and particulate phases is modeled by adding source terms in the gas momentum and energy equations. These terms represent the momentum and energy exchanges between the two phases.

The turbulence of the flow is modeled by using a k-ε based model derived from the instantaneous Navier-Stokes equations, using a mathematical technique called the "renormalization group" (RNG) methods. The analytical derivation result in a turbulence model with constants that differ from that of the standard k-ε model, and with additional terms and functions in the transport equations of k and ε . A comprehensive description of the RNG theory and its application to turbulence can be found in Ref 13.

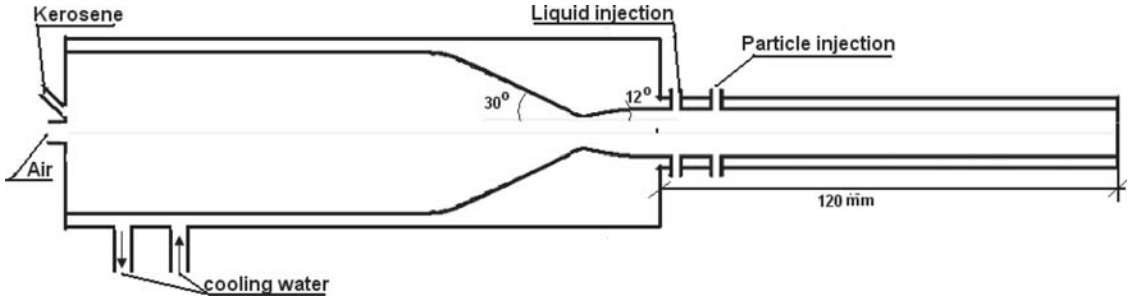

Fig. 1 Schematic diagram of LTHVAF spraying gun and nozzle

Table 1 Parameters and initial conditions for LTHVAF spraying

Parameters	Initial conditions
Fuel/Air flow rate (Kerosene/(O_2N_2)	2.5/8/25 L/h
Powder carrier gas (N_2)	5L/h
Powder feed rate	4 g/s
Spray distance	200 mm
Injected liquid pressure	3.5 MPa
Particle initial velocity	20 m/s
Particle temperature	300 K

$$\frac{\partial \rho}{\partial t} + \frac{\partial (\rho u_j)}{\partial x_j} = 0 \qquad \text{(Eq 1)}$$

$$\frac{\partial}{\partial t}(\rho k) + \frac{\partial}{\partial x_i}(\rho k u_i) = \frac{\partial}{\partial x_i}\left[\alpha_k \mu_{eff} \frac{\partial k}{\partial x_j}\right] + G_k + G_b - \rho\varepsilon - Y_M + S_k \qquad \text{(Eq 2)}$$

$$\frac{\partial}{\partial t}(\rho \varepsilon) + \frac{\partial}{\partial x_i}(\rho \varepsilon u_i) = \frac{\partial}{\partial x_i}\left[\alpha_\varepsilon \mu_{eff} \frac{\partial \varepsilon}{\partial x_j}\right] + C_{1\varepsilon}\frac{\varepsilon}{k}(G_k + C_{3\varepsilon}G_b) - C_{2\varepsilon}\rho\frac{\varepsilon^2}{k} - R_\varepsilon + S_\varepsilon \qquad \text{(Eq 3)}$$

In Eq 1 to 3, G_k is the generation of turbulent kinetic energy for the mean velocity gradient, G_b is the generation of turbulent kinetic energy due to buoyancy, Y_M is the contribution of the fluctuating dilatation to the overall dissipation rate. $C_{1\varepsilon}$, $C_{2\varepsilon}$, and $C_{3\varepsilon}$ *are constants.* σ_k and σ_ε are the turbulent Prandtl numbers for k and ε, respectively. S_k and S_ε are user-defined source terms.

The set of governing equations is solved using the CFD Code Fluent V6.0 (Ref 14).

2.2 Particle and Droplet Dynamics Equation

The velocity of the gas jet is maximal at the exit of the atomizer nozzle and, then, decreases with distance as its momentum is transferred to the droplet phase and to the ambient gas.

When a spherical particle or droplet is accelerated or decelerated during its motion in a fluid, the Newton's second law is expressed by:

$$\rho_d V_d \frac{du_d}{dt} = V_d(\rho_d - \rho_g)g - \frac{1}{2}\rho_g A_d C_d |u_d - u_g|(u_d - u_g) \qquad \text{(Eq 4)}$$

Equation 4, which assumes that only the inertia, gravitation, and the drag forces determine the droplet and particle motion, makes it possible to determine the variation of droplet and particle velocity with the distance from the atomization and injection points, respectively.

2.3 Particle and Droplet Energy Equation

A simple heat balance in the boundary layer surrounding the particle and droplet is used to calculate the time-variation of the particle and droplet temperature:

$$m_p c_p \frac{dT_p}{dt} = hA_p(T_\infty - T_p) + \varepsilon_p A_p \delta(\theta_R^4 - T_p^4) \qquad \text{(Eq 5)}$$

The first term in the right-hand side of Eq 5 corresponds to the heat exchanged with the gas phase by conduction and convection, whereas the second term represents the heat exchanged by radiation. It is supposed that the temperature of the particle is spatially uniform at any instant.

Equation 5 is solved by using an approximate, linearized form assuming that the variation of the particle temperature over one time step is low:

$$m_p c_p \frac{dT_p}{dt} = A_p\{-[h + \varepsilon_p \delta T_p^3]T_p + [hT_\infty + \varepsilon_p \delta \theta_R^4]\} \qquad \text{(Eq 6)}$$

As the particle trajectory is computed, Eq 6 is integrated to obtain the particle temperature at the next time step yielding to:

$$T_p(t + \Delta t) = \alpha_p + [T_p(i) - \alpha_p]e^{-\beta_p \Delta t} \qquad \text{(Eq 7)}$$

where Δt is the integration time step and:

$$\alpha_p = \frac{hT_\infty + \varepsilon_p \delta \theta_R^4}{h + \varepsilon_p \delta T_p^3(t)} \qquad \text{(Eq 8)}$$

$$\beta_p = \frac{A_p[h + \varepsilon_p \delta T_p^3(t)]}{m_p c_p} \qquad \text{(Eq 9)}$$

Finally, the heat lost or gained by the particle as it traverses each computational cell appears as a source or sink of heat in the subsequent calculations of the gas phase energy equation.

When the droplet temperature reaches the boiling point, the

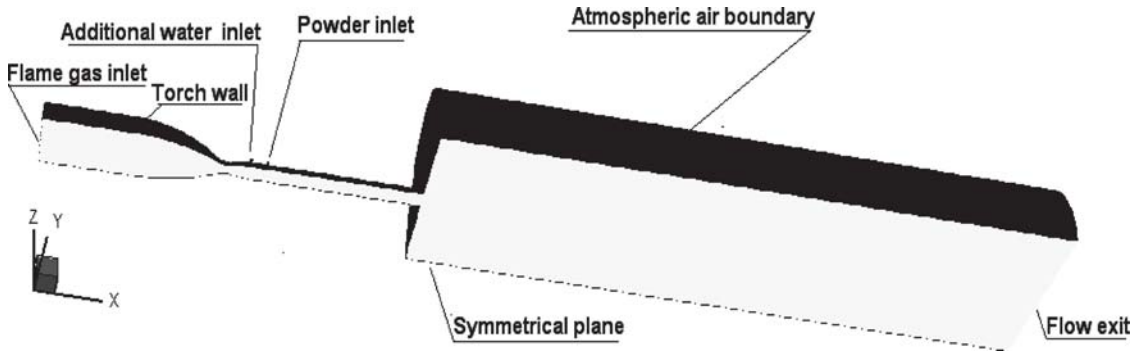

Fig. 3 Schematic diagram of LTHVAF spray process and computational domain

following equation is applied to predict the variation of the droplet size:

$$\frac{dd_p}{dt} = \frac{4k_\infty}{\rho_p c_{p,\infty} d_p} \cdot (1 + 0.23\sqrt{\mathrm{Re}_d}) \ln\left[1 + \frac{c_{p,\infty}(T_\infty - T_p)}{h_{fg}}\right] \quad (10)$$

Equation 10 has been derived assuming a steady flow at constant pressure. When the radiation heat transfer is active, a slight modification is used in Eq 10, assuming that the droplet temperature is constant. This yields to Eq 11:

$$-\frac{dd_p}{dt} = \frac{2}{\rho_p h_{fg}}\left[\frac{k_\infty \mathrm{Nu}}{d_p}(T_\infty - T_p) + \varepsilon_p \delta(\theta_R^4 - T_p^4)\right] \quad \text{(Eq 11)}$$

In the absence of radiation, the predictions from Eq 10 and 11 are identical as long as the argument of the logarithm is close to unity (Ref 14).

The variation in droplet diameter is taken into account in the trajectory equation (Eq 4) and the energy required for droplet vaporization is added as a sink term in the energy equation of the gas phase as it absorbs a part of the gas flow energy.

2.4 Boundary Conditions

The boundary conditions for the LTHVAF flow numerical model are given in Table 2 and Fig. 3.

2.5 Validation of Model Predictions

During spraying, the flame structure outside the spray gun is observed by using photographic methods. In addition, the particle and gas temperature are measured using a Raynger 3i IR pyrometer (Raytek Corporation, Santa Cruz, CA).

3. Results and Discussion

3.1 Effect of Liquid Volume Flow Rate on Gas Flow Characteristics

Figure 4 shows the variation of gas velocity and temperature with the flow rate of water. The injection of the liquid changes drastically the temperature and velocity of the flame. However, the flame is still supersonic.

When the supersonic flame is formed after the nozzle, an appropriate liquid injection can be propitious to the spraying process as it enables some control on the gas characteristics. However, if the liquid flow rate is too high it can cause the extinguishing of flame.

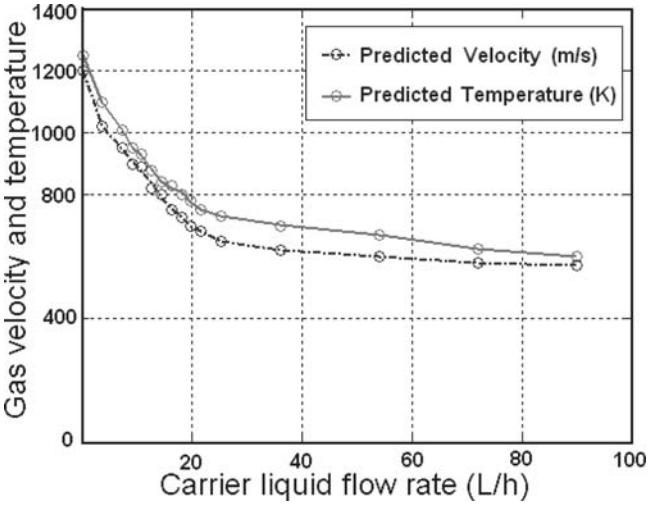

Fig. 4 Variation of gas velocity and temperature with water flow rate

Table 2 Boundary conditions

Parameter, unit	Gas inlet	Water inlet	Particle inlet	Wall	Far-field
Gas flow, kg/s	0.024	0.9	0.8	…	…
Pressure, MPa	0.85	0.35	0.35	…	0.1
Temperature, K	2200	300	…	300	400
Heat flux, W/m^2	…	…	…	5	…

The numerical results show that an increase in the water flow rate brings about a decrease in the flame temperature and velocity. In the LTHVAF spray process, the optimal operating conditions correspond to a water flow of about 20 and 30 kg/h. Under these conditions, the gas temperature is in the order of 600 to 700 K and the gas velocity of 700 to 800 m/s. It should be noticed that the spraying characteristics are then close to that of the cold spray technology.

The predicted gas field of the LTHVAF process is shown in Fig. 5. At the liquid entrance, the low-temperature liquid water

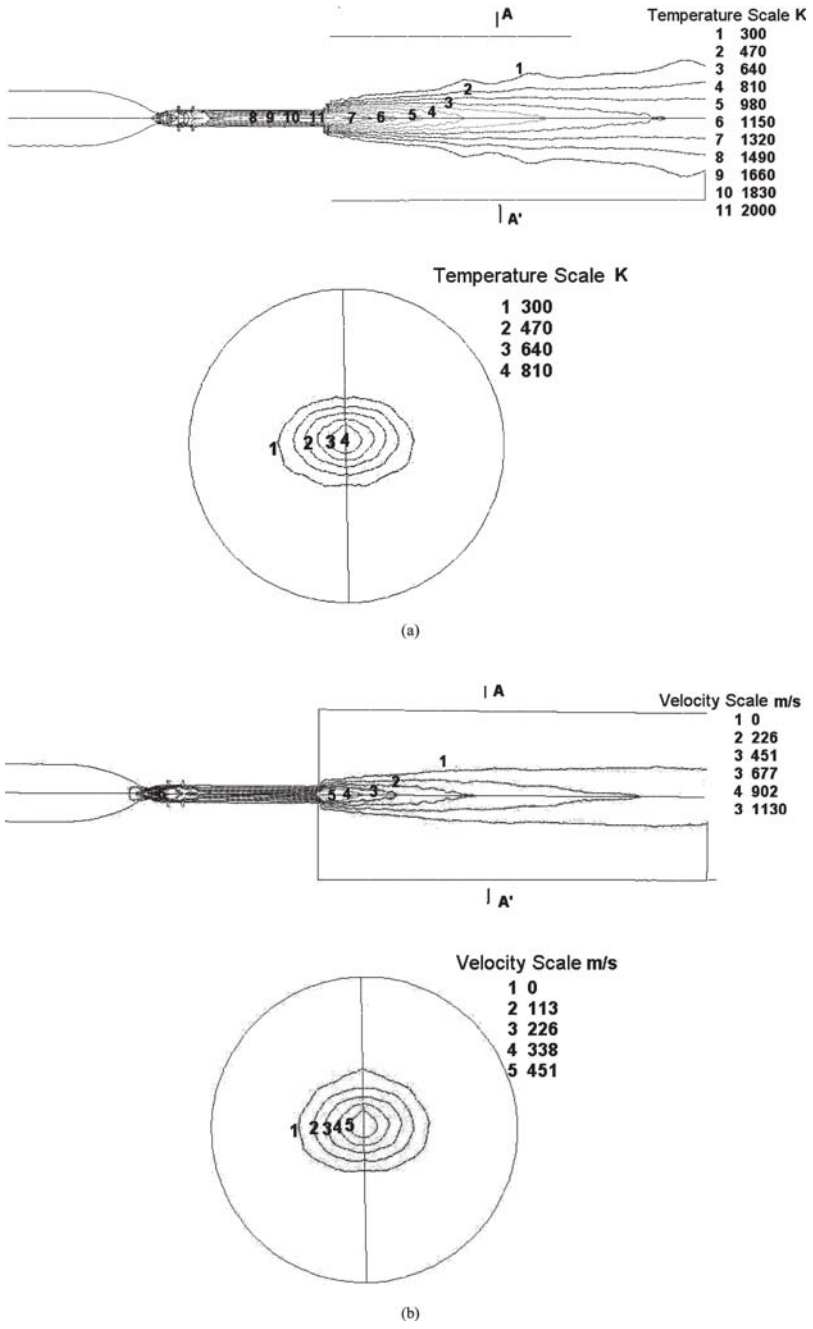

Fig. 5 Axial velocity and temperature contours of the flame plume in the plane of symmetry and cross section (A-A′): (a) velocity contours; (b) temperature contours

exchanges energy with the flame and drastically affects the gas parameters. The flame characteristics are gradually affected from the edge to the center. Compared with the gas velocity, the injected water radial velocity is very small but the mixing with the gas phase will be favored by the engulfment process due to turbulence.

3.2 Effect of Particle Size on Particle Behavior

Figure 6 shows the particle size distribution and the particle in-flight behavior. The calculations make it possible to determine the optimal liquid flow rate for a specific particle velocity.

The particle size distribution is defined by fitting the actual size distribution data to a Rosin-Rammler distribution (Ref 14); the particle size range is divided into a set of discrete size ranges, each defined by a single value.

When the water mass flow rate is about 20 kg/h, the Ni and Cu particle temperature (Fig. 6b) are higher than 900 K for particles with diameter less than 20 μm. Indeed, the particle track may separate with the water droplet tracks as the particle density is much higher than that of water. As expected, the particle temperature decreases when the gas temperature decreases.

At the gun exit, the velocity and temperature of Cu particles

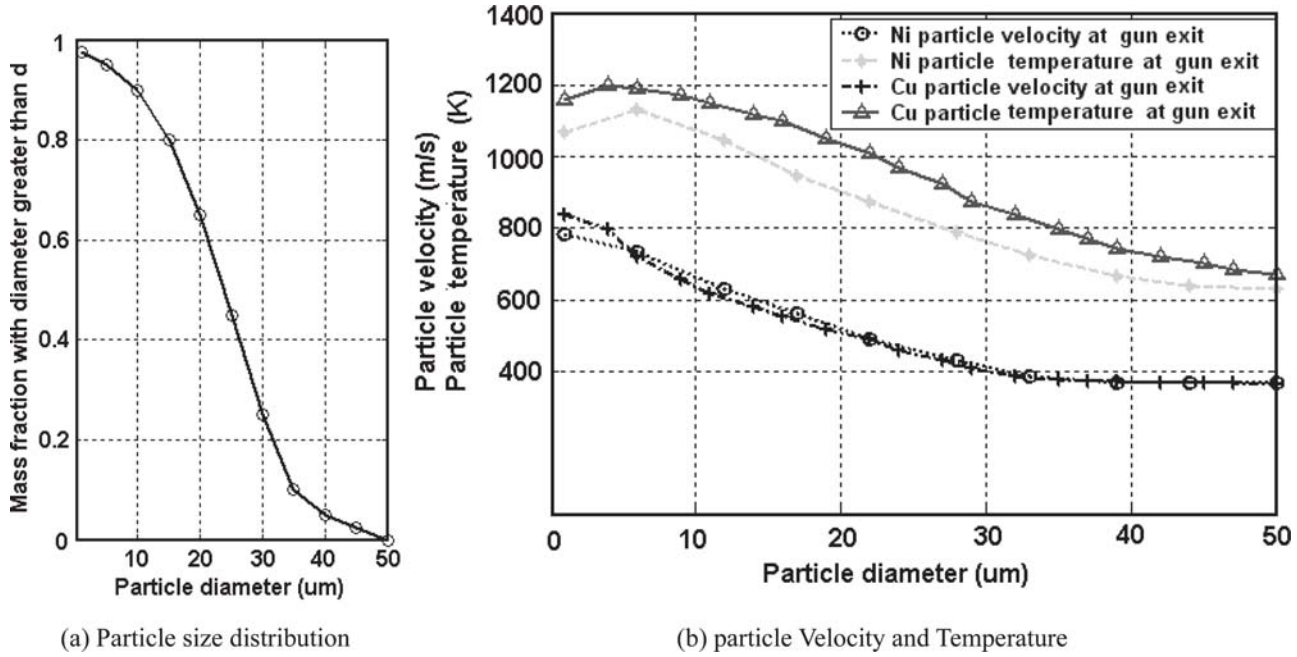

Fig. 6 (a) Copper and nickel particle size distributions and (b) behavior at gun exit.

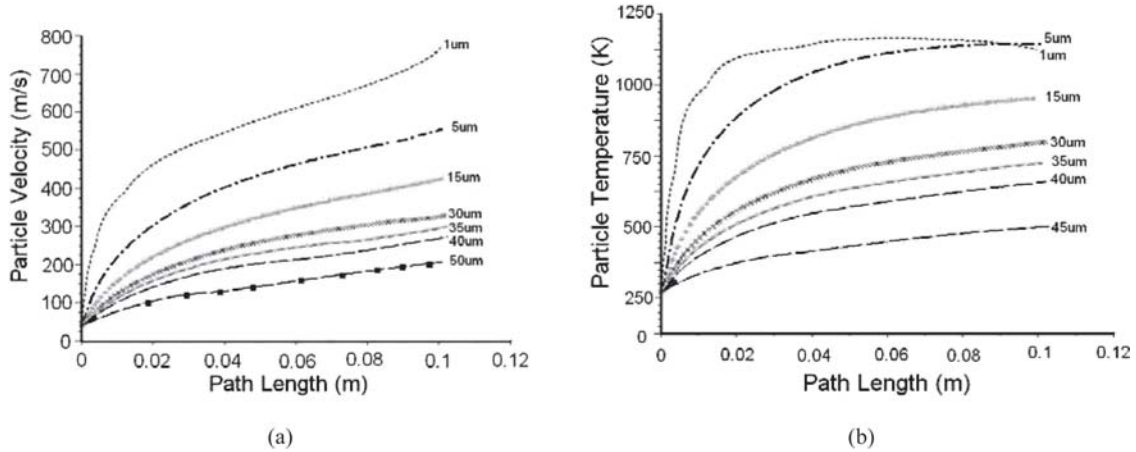

Fig. 7 In-flight Cu particle behaviors along the axial distance: (a) velocity; (b) temperature

with diameter ranging between 1 and 50 μm, vary between 700 and 300 m/s and between 900 and 400 K, respectively.

The particle in-flight behaviors in the gun are shown in Fig. 7. During the process, the atomized water is vaporized. However, the metal particles can be easily injected up to the flame core due to a higher density. The gas temperature and velocity in the flame core are higher than that of particles and, thus, the particles can be heated and accelerated.

The predictions show that the smaller particles are accelerated to a higher velocity but slow down rapidly due to their smaller momentum inertia, whereas the larger particles are accelerated with some difficulty. The same tendency is observed regarding the effect of particle size on its thermal history.

When the particles and water droplets are injected in the flame, the gas fields change, as shown in Fig. 8. The z-direction characteristics of the flame gas become asymmetrical and the gas temperature is lower in the planes where the particles and droplets are injected.

In the spray process, the discrete phases enter the flame gas core step by step. The metal particles can get the necessary en-

Table 3 Material melting point

Material	Melting point, K
Sn	503
Pb	600
Zn	692
Mg	923
Al	933

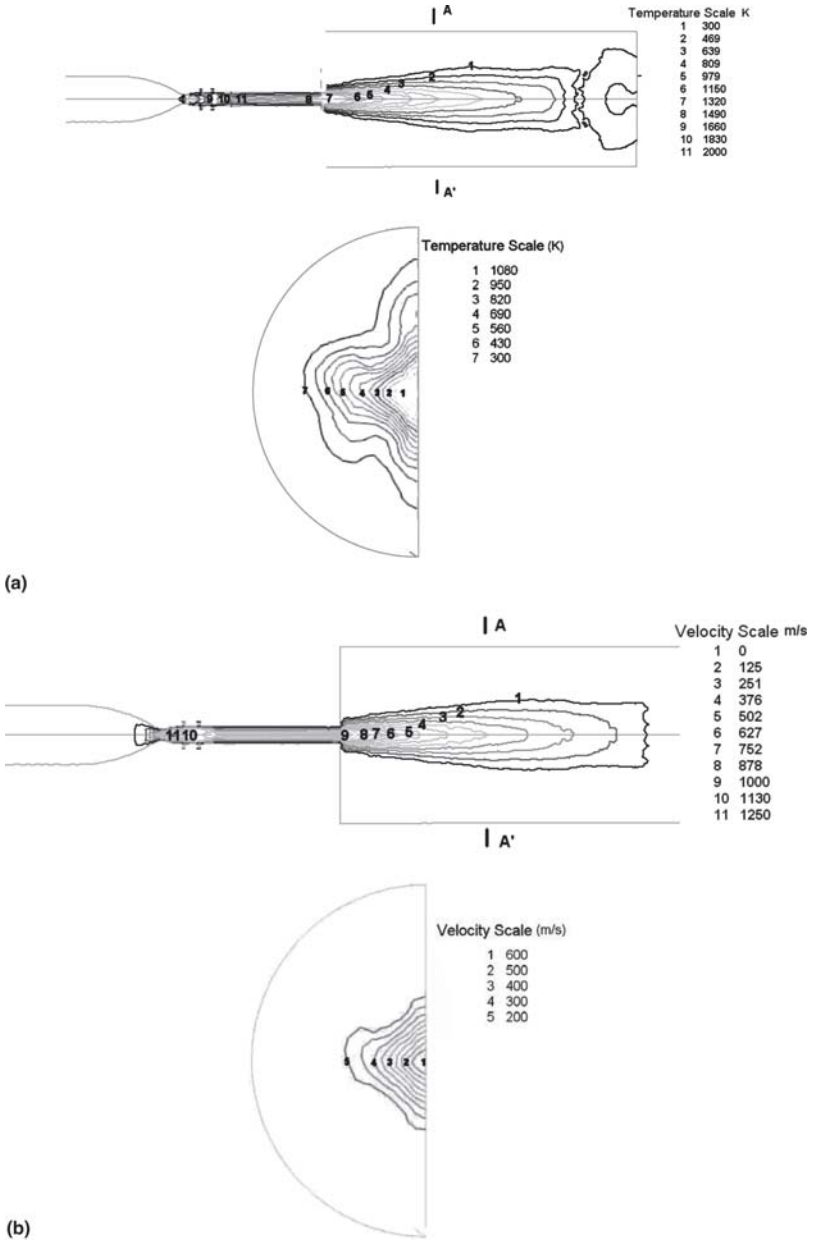

Fig. 8 Contours of gas characteristics when metal particles are injected: (a) temperature contours; (b) velocity contours (m/s)

ergy for melting and acceleration. So, the required relationships between the particle diameter and physical characteristics with the flame velocity, temperature, and the gun design are achieved.

3.3 Experiment Evaluation

In this study, the gas temperature is determined from the melting of metal rods put in the flame. The melting points of some materials are listed in Table 3. Table 4 shows the predicted and measured gas and particle temperature for various operating conditions. The agreement between predictions and measurement is acceptable.

3.4 Manufacturing Coatings by the LTHVAF Spraying Process

Copper and nickel coatings are manufactured under the optimal operating conditions predicted by the numerical simulations. The substrate is medium carbon steel and the coating thickness is 0.3 mm. The microphotographs and XRD graphs of the Cu and Ni coatings are shown in Fig. 9(a) and (b), respectively.

The coatings are dense with very low porosity and oxide content. Only small holes in the Cu coatings and some cracks in the Ni coatings are visible. Indeed, the particle temperature does not exceed 900 K and the particles are not subjected to oxidation in the spray process. Therefore, the coatings composition is iden-

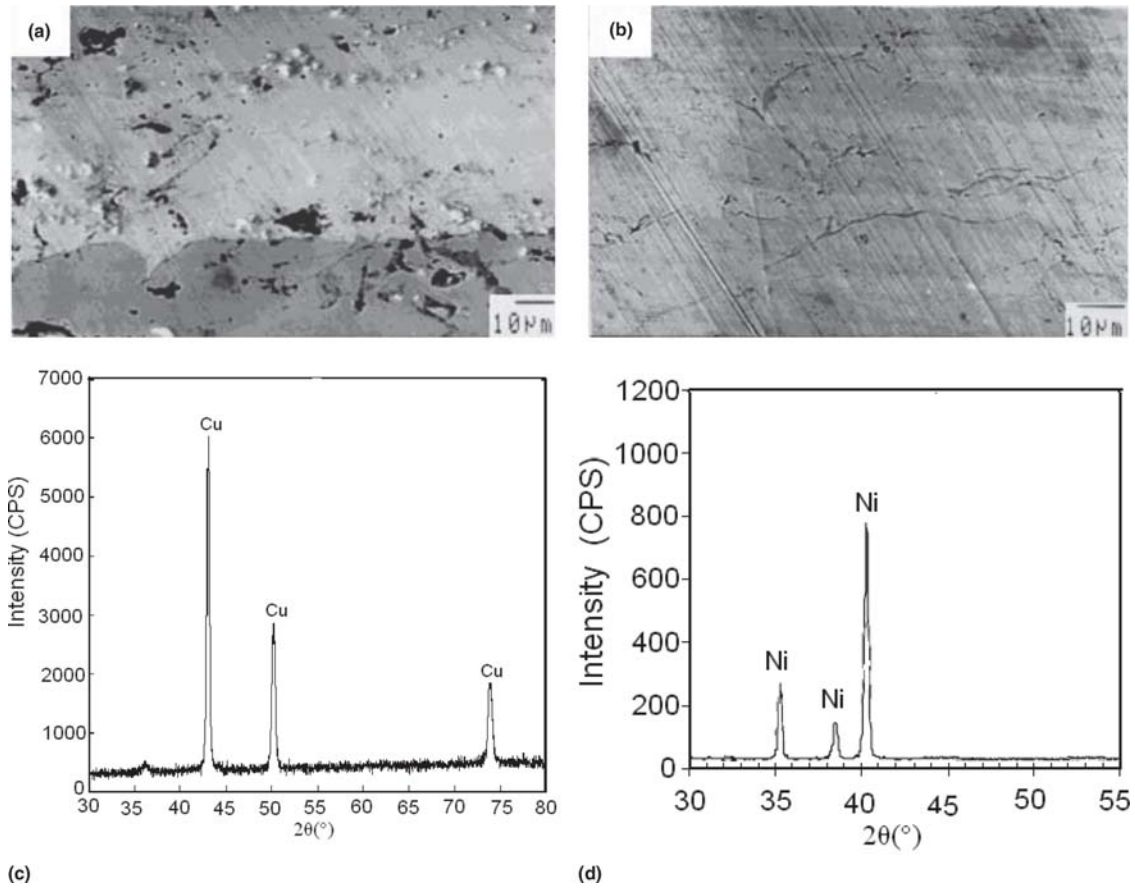

Fig. 9 Microphotographs of coating surface and XRD graphs of Cu and Ni coatings: (a) and (c) Cu coatings; (b) and (d) Ni coatings

Table 4 Comparison of predicted and measured gas temperature at gun exit

Airflow, kg/s	Kerosene flow rate, kg/s	Liquid flow rate, L/h	Gas temperature, K	
			Simulations	Experiments
0.02248	0.00152	50	755	520 ± 50
0.02248	0.00152	20	780	640 ± 80
0.02248	0.00152	18	800	670 ± 94
0.02248	0.00152	10	975	846 ± 83
0.02248(a)	0.00152	0	1250	1310 ± 87

(a) HVAF state of the HVO/AF spray

Table 5 Bond strength of Cu coatings

Sample number	Maximum load, MPa	Mean load, MPa
11	8.01*	…
12	17.50	…
13	18.14	16.43
14	19.68	…
15	18.82	…

tical to that of the original powders (Fig. 9). In addition, when the particle velocity exceeds a critical value, the coatings will be formed easily.

The Cu coating bonding strength measured by the Instron1195 electron drag testing machine (Ref 15) is shown in Table 5. The mean bond strength of the coatings is 16.43 MPa. The fracture always occurs at the interface between the coatings and substrate. It shows that the coatings are characterized by little oxidation, low residual stresses, and high cohesion structure

4. Summary and Conclusions

In this paper, a three-dimensional model of the LTHVAF spray process with simultaneous injection of water droplets and metal particles has been presented.

The main conclusions drawn from the current study are:

- The flame temperature and velocity are affected by the injection of the liquid in the combustion gas. A water film

forms at the edge of the flame and enters progressively in the gas. Therefore, a conical region is formed. The numerical results show that the appropriate flame characteristics are achieved when the water flow rate is about 20 to 30kg/h. The gas temperature and velocity is, then, about 600 to 700 K and 700 to 800 m/s, respectively. These characteristics are close to that of the cold spray process.

- The calculations of particle behavior in the gas flow show that the velocity and temperature of Cu and Ni particles of 1 to 50 μm range between 700 and 300 m/s, and 900 and 400 K, respectively. The Cu and Ni coatings exhibit low oxide content, low residual stresses, high deposition rates, and good coating bond strength.

In conclusion, the work presented in this paper makes it possible to develop a comprehensive model of the three-dimensional characteristics of a LTHVAF spray process with the simultaneous injection of metal particles and water droplets. It proposes a new process with characteristics close to that of the cold spray process.

References

1. W. Roger, Kaufold, A.J. Rotolico, J. Nerz, Burton, A. Kushner, Deposition of Coatings Using a New High Velocity Combustion Spray Gun, *Therm. Spray Research and Applications, Proc. of 3rd National Therm. Spray Conf.,* C.C. Berndt, Ed., May 20-25, ASM International, 1990, p 561-574
2. B. Zha, H. Wang, X. Su, Structure and Property of WC-17Co Coatings Sprayed by HVO/AF, *Thermal Spray 2003: Advancing the Science & Applying the Technology,* C. Moreau and B. Marple, Ed., May 5-8, ASM International, 2003, p 837-839
3. H. Wang, B. Zha, X. Su, High Velocity Oxygen/Air Fuel Spray, *Thermal Spray 2003: Advancing the Science & Applying the Technology,* C. Moreau and B. Marple, Ed., May 5-8, ASM International, 2003, p 789-791
4. H. Wang, B. Zha, Research of High Velocity Oxygen-Air Fuel Spray, *Proceedings of the 3rd International Conference on Surface Engineering,* October 10-13 (ChengDu, China), 2002, p 166-168
5. N. Anatolii, Papyrin, Cold Spray Process for Cost-Sensitive Application, *High Performance Metallic Materials for Cost Sensitive Applications,* F.H. (Sam) Froes, E. Chen, R.R. Boyer, E.M. Taleff, L. Lu, D.L. Zhang, C.M. Ward-Close, and D. Elizer, Ed., TMS, 2002, p 137-149
6. J. Karthikeyan and C.M. Kay, Cold Spray Technology: An Industrial Perspective, *Thermal Spray 2003: Advancing the Science & Applying the Technology,* C. Moreau and B. Marple, Ed., May 5-8, ASM International, 2003, p 117-121
7. K. Sakaki and Y. Shimizu, Effect of the Increase in the Entrance Convergent Section Length of the Gun Nozzle on the High-Velocity Oxygen Fuel and Cold Spray Process, *J. Therm. Spray Technol.,* 2001, **10**(3), p 487-496
8. B. Zha, H. Wang, and K. Xu, Microstructure and Property of LTHVOF Sprayed Copper Coatings, *International Thermal Spray Conference & Exposition,* E. Lugscheider, Ed., May 2-4, 2005
9. J. Karthikyan and C.M. Kay, Cold Spray Nanostructured WC-Co, *Thermal Spray 2001: New Surface for a New Millennium,* C.C. Berndt, K.A. Khor, and E.F. Lugscheider, Ed., May 28-30, 2001 (Singapore), ASM International, 2001, p 383-387
10. N.S. Mahesh, J. Mendonca, M.K. Muralidhara, B.K. Muralidhara, and C. Ramachandra, Modeling of droplet dynamic and thermal behavior during spray deposition, *Bull. Mater. Sci.,* 2003, **26**(3), p 355-364
11. C.M. Hakett, The Influence of Nozzle Design on HVOF Spray Particle Velocity and Temperature, *Proceeding of the National Thermal Spray Conference,* September 11-15 (Houston, Texas), 1995, p 135-140
12. P.E. Nylén and R. Bandyopadhyay, Computational Fluid Dynamics Analysis of Gas and Particle Flow in Flame Spraying, *Proceeding of the 1st International Thermal Spray Conference,* C.C. Berndt, Ed., May 8-11, 2000, p 237-245
13. D. Choudhury, *Introduction to the Renormalization Group Method and Turbulence Modeling*. Fluent Inc. Technical Memorandum TM-107, 1993.
14. FLUENT 6.0 Documentation Fluent Inc. *2001-11-29*
15. B. Zha, H. Wang, and X. Su, Structure and Property of WC-17Co Coatings Sprayed by HVO/AF, *Thermal Spray 2003: Advancing the Science & Applying the Technology,* C. Moreau and B. Marple, Ed., May 6-8, ASM International, 2003, p 837-839